Quasi-Gaussian Multibeam Solar Laser Station for a Megawatt Solar Furnace

Hugo Costa, Joana Almeida, Dawei Liang*, Bruno D. Tibúrcio, Dário Garcia, Miguel Catela and Cláudia R. Vistas

CEFITEC, Departamento de Física, Faculdade de Ciências e Tecnologia, Universidade NOVA de Lisboa, 2829-516 Caparica, Portugal

Abstract: An alternative multirod solar side-pumping concept for the production of multiple quasi-Gaussian beams is proposed. This scheme was based on the One-Megawatt solar furnace in Odeillo, France, which collected and concentrated the solar light into a multilayered pyramidal pumping cavity placed at the focal zone. Each layer was comprised of a square array of four laser heads, each composed of a biconic surface that reflected the solar rays towards a Nd:YAG rod fixed inside a fused silica flow tube. A pyramidal reflector was placed inside the pumping cavity to close it and maximize the harness of solar energy. Compared to the previous multibeam solar laser station design for the same solar furnace, considerable alleviation of thermal lensing effects was achieved with the present approach, allowing the improvement of the laser beam quality factors and, consequently, the possibility of a 32-laser-beam generation, each with a quasi-Gaussian profile. For this case, 9.44 kW total laser power was calculated. Additionally, 20.01 kW total multimode laser power was numerically determined, which corresponds to a 10.93 W/m^2 collection efficiency and a 2.0% solar-to-laser power conversion efficiency.

Keywords: Solar laser, solar pumping, multirod, Nd:YAG, solar furnace.

1. INTRODUCTION

The solar-pumped laser is considered one of the most promising technologies in renewable energy research. The direct excitation of lasers by natural sunlight provides a cost-effective solution to free coherent optical radiation generation. Furthermore, the complete dismissal of artificial pumping sources, along with their associated electrical power consumption and conditioning equipment, constitutes an added value. Solar-pumped lasers can be important in remote locations where sunlight is abundant, especially where extended run times, compactness, reliability, and efficiency are required. This makes them quite enticing for space-based applications, including atmospheric and ocean sensing, free-space laser communications, space-to-earth power transmission and asteroid deflection [1–3], while also having great potential for terrestrial applications [4,5].

The first report of a solar-pumped laser occurred in 1963 by Kiss *et al*. [6], not long after the invention of the laser [7]. With this novel technological achievement, researchers focused their attention towards developing new ways to improve solar laser performance by experimenting with a variety of optical components and laser materials. However, there was little progress after Young succeeded in demonstrating the first 1 W continuous-wave Nd:YAG solar laser emission, in 1966 [8]. 18 years later, Arashi *et al*. [9] attained 18 W by side-pumping a Nd:YAG rod. This record value of solar output power would later be broken by Weksler and Shwartz [2], who, in 1988, produced 60 W using a rod of the same material and a two-dimensional secondary compound parabolic concentrator. Since the late 1990s, maximizing collection efficiency – defined as solar laser output power per unit of primary concentrator area [10] – became the one of main goals in solar laser research [10–20]. For this figure of merit, the record currently sits at 32.5 W/m^2, achieved in 2018, with the end-side-pumping of a Cr:Nd:YAG ceramic rod by a 1.0 m^2 effective collection area heliostat-parabolic mirror concentration system [12].

Exposing a single laser rod to high pumping radiation can cause significant thermal lensing and thermal stress effects [21]. Even though the reduction of its diameter makes it more thermally resistant, it can severely limit the laser power production. In order to overcome this issue, solar pumping concepts using multiple rods have been proposed, promoting the distribution of concentrated radiation amongst them [22–27]. In 2008, a five-rod scheme with a side-pumping configuration was designed for the One-Megawatt solar furnace of Materials Science Institute of Uzbek Academy of Sciences, predicting a laser power production of 1.5 kW and a solar-to-laser power conversion efficiency of 1.3% [22]. In 2020, a multirod solar laser station was proposed to study the feasibility of these systems for solar energy research in solar furnaces of a larger scale [27]. By employing the One-Megawatt solar furnace (MWSF) of Procédés, Matériaux et Energie Solaire – Centre National de la Recherche Scientifique (PROMES-CNRS) as the collection and concentration system, twelve rods were side-pumped after a solar homogenizer received most of the concentrated solar radiation and reshaped the near-Gaussian solar pump light distribution at its input

*Address correspondence to this author at the CEFITEC, Departamento de Física, Faculdade de Ciências e Tecnologia, Universidade NOVA de Lisboa, 2829-516 Caparica, Portugal; E-mail: dl@fct.unl.pt

E-ISSN: 2410-2199/21

face into a nearly uniform one at its output end face. Total multimode solar laser power of 22.84 kW was numerically determined, which corresponded to a 12.48 W/m^2 collection efficiency and a 2.28% solar-to-laser power conversion efficiency. Nevertheless, this concept exhibited strong thermal lensing in each rod, impairing the laser beam quality.

To significantly alleviate the thermal lensing effects of solar laser systems in solar furnaces of large scale, an alternative multirod/multibeam solar laser pumping concept is presented in this paper. The MWSF of PROMES-CNRS constitutes the collection and concentration system for solar radiation. At the focal zone, an eight-layered structure with pyramidal shape was positioned, within which a total of 32 Nd:YAG rods were side-pumped. A pyramidal reflector was placed inside the large pump cavity to close it and help redirect the solar rays towards the rods. This scheme enabled efficient production of 20 kW-class total multimode laser power, corresponding to a 10.93 W/m^2 collection efficiency and a 2.0% solar-to-laser power conversion efficiency, with the latter representing a 1.54 times enhancement over that of the scheme with the MWSF in Uzbekistan [22]. More importantly, it also ensured significant alleviation of the thermal lensing effects and, thus, the improvement of the laser beam quality factors with the possibility of generating 9.44 kW total laser power from 32 laser beams with quasi-Gaussian profiles, which would not have been possible with the previously mentioned scheme with the MWSF of PROMES-CNRS [27]. All design parameters were numerically optimized on both Zemax® nonsequential ray-tracing and laser cavity analysis and design (LASCAD™) software.

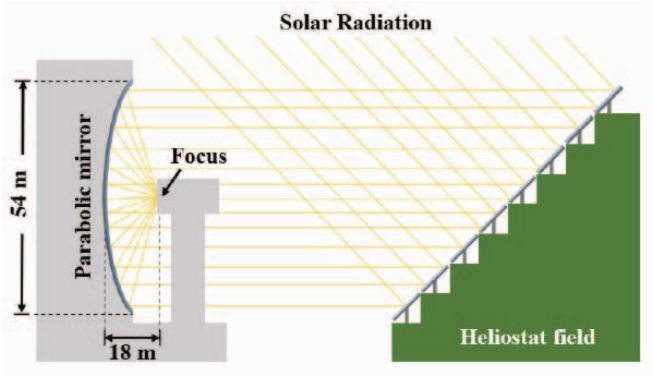

Figure 1: Simplified schematic of the MWSF facility in PROMES-CNRS.

2. QUASI-GAUSSIAN MULTIBEAM SOLAR LASER STATION

2.1. Solar Energy Collection and Concentration System

The MWSF of PROMES-CNRS is composed by 63 heliostats with a total surface area of 2835 m^2 that collect and redirect sunlight towards a 1830 m^2 facetted truncated parabolic mirror with 18 m focal length, installed on the north face of the 8th floor building [28]. The parabolic mirror then focus 1 MW of solar power into an 80 cm diameter near-Gaussian spot, reaching a peak flux value beyond 10 W/mm^2 [29]. In Figure **1**, a schematic depiction of the collection and concentration system is presented.

2.2. Pyramidal-Shaped Structure with Multiple Nd:YAG Solar Laser Heads

An eight-layered pyramidal structure was placed at the focal zone of the parabolic mirror (Figure **2**). Each layer was comprised of a square array of four laser

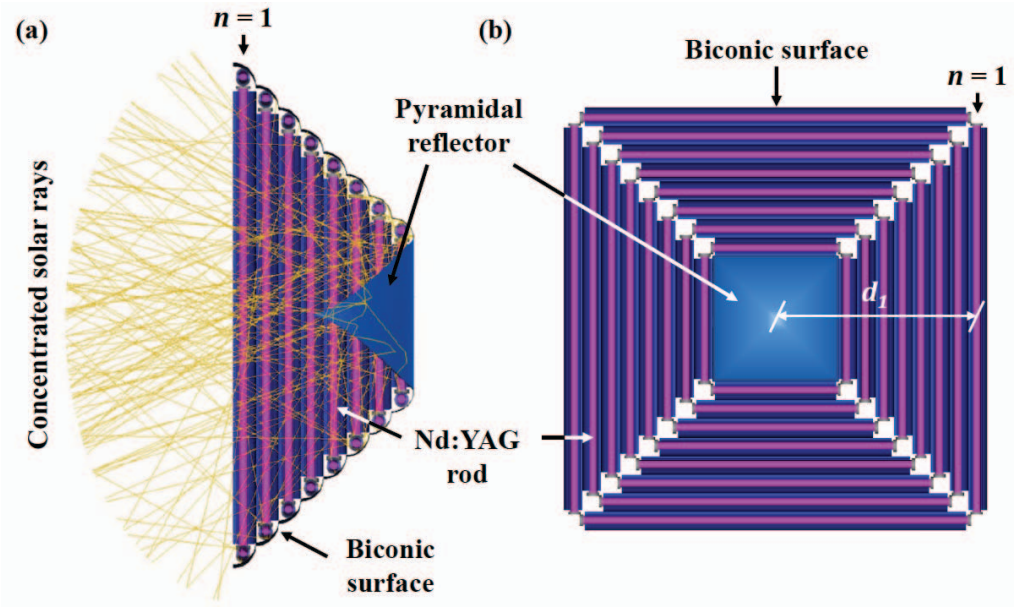

Figure 2: (**a**) Cross-sectional and (**b**) top-view of the multilayered pumping cavity. 𝑛 represents the layer number. d_1 (= 240 mm) is the distance between the rods of the layer closest to the focal zone (𝑛 = 1) and the central axis of the main structure.

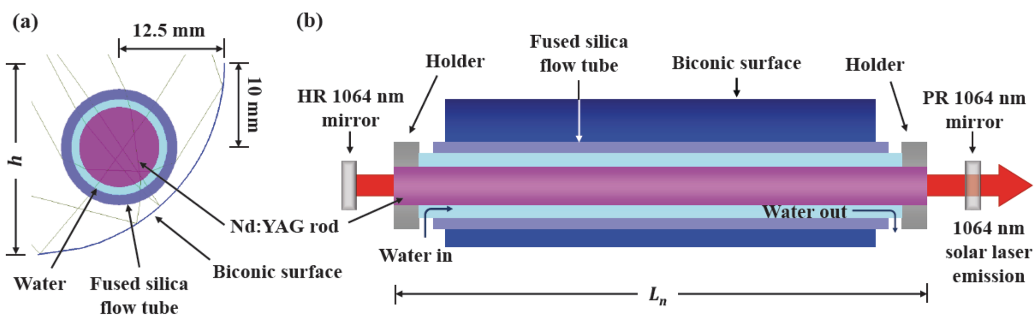

Figure 3: (**a**) Cross-sectional and (**b**) top-view of one of the single laser heads of the scheme. The highly reflective (HR) 1064 nm and the partially reflective (PR) 1064 nm mirrors, along with the Nd:YAG rod, form the laser resonator. h is the height of the biconic surface and L_n is the rod length.

heads, which, in turn, were composed of a biconic surface that reflected the incoming solar light towards a Nd:YAG crystal rod, fixed inside a fused silica flow tube, as illustrated in detail in Figure **3**. A pyramidal reflector, imported from AutoCAD®, was placed inside the main structure to close it (Figure **2**). It had a 150.0 mm base width and a 102.3 mm height. With the use of the Loft command in AutoCAD®, the reflector's lateral faces were designed to present a slight curvature, facilitating the redirection of solar rays towards the rods. A 95% reflectivity was considered for the inner walls of the biconic surfaces and the lateral faces of the pyramidal reflector.

Each biconic surface (Figure **3**), placed 12.5 mm away from the center of the rod and 10 mm above it, had a radius of curvature R_{bc} of 22.75 mm and height h of 22.74 mm. A conic constant k = 0 was considered for the design. The length of each biconic surface was always 16 mm shorter than the rod of the same laser head to allow mechanical fixation of both fused silica flow tube and laser rod.

Nd:YAG was the chosen laser material for highly intense solar pumping due to the remarkable spectroscopic properties of the active laser [30], its availability, relatively low cost and good thermomechanical properties that make it resilient and durable [2]. Each Nd:YAG rod was cooled with water flowing inside the fused silica flow tube along most of its longitudinal surface, with 4 mm on each side of the rod used for mechanical fixation by two holders. Each flow tube had a 1.25 mm wall thickness, while its inner diameter was calculated by considering a cross-section area of 30 mm^2 used exclusively for cooling water circulation. Moreover, its length was 12 mm shorter than the rod inside of it, allowing the presence of 2 mm spacings between each flow tube end and the rod holders for water entrance and exit. The cooling water played an important role in temperature regulation due to its high thermal conductivity and specific heat, as well as low viscosity.

The length of the Nd:YAG rods from each layer (n) was dictated by the distance between the rods and the central axis of the main structure, D_n. The four rods from the layer closest to the focal zone (n = 1) were located D_n = 240 mm away from the central axis of the main structure, as shown in Figure **2b**. For the following layers, D_n was determined through Equation 1,

$$D_n = D_{pre} + R_{bc} + R_{bc}\cos\left[\sin^{-1}\left(h/R_{bc}\right)\right], \tag{1}$$

with D_{pre} being the distance between the rods of the previous layer and the central axis of the structure. As aforementioned, R_{bc} and h are the radius of curvature (= 22.75 mm) and height (= 22.74 mm) of the biconic surface, respectively. Finally, the rod length L_n was the rounded value given by

$$L_n = 2D_n - c \tag{2}$$

Here, c (= 13 mm) is a fixed value required to guarantee that the rods would not intersect with each other in the design or hamper the laser emission from the other laser heads.

The laser resonator for each laser rod was formed by two opposing mirrors aligned with the optical axis of the active medium. One mirror had a highly reflective (HR) coating at the 1064 nm laser emission wavelength, whereas the other one had a partially reflective (PR) coating at 1064 nm, enabling the solar laser emission.

3. NUMERICAL MODELING OF THE MULTIBEAM SOLAR LASER STATION

3.1. Modeling of the Optical Design Parameters through Zemax® Software

During optimization of the design parameters in Zemax®, the standard solar spectrum for one-and-a-half air mass [31] was used as the reference data for consulting the spectral irradiance for each wavelength of the solar spectrum. Both terrestrial solar irradiance of 1000 W/m^2 in Odeillo, France, and the 0.27° solar half-angle were also considered. The effective pump power of the light source took into account the 16% overlap between the Nd:YAG

absorption and the solar emission spectra [32]. The 22 peak absorption wavelengths and their respective absorption coefficients for 1.0 at% Nd:YAG laser medium, in addition to the absorption spectra and wavelength-dependent refractive indices of fused silica and water, were also included in the glass catalogue data.

A detector volume, divided into 80000 voxels, was used for each rod for ray-tracing analysis of the absorbed pump power within the laser media and respective pump distribution. The absorbed pump power was calculated through the sum of absorbed pump radiation in every voxel. The number of analysis rays and voxels were adjusted in order to produce more accurate results and better image resolution of the detector, while taking into consideration their influence on the total time required for each simulation. Figure **4** shows the absorbed pump flux distribution in the central transversal and longitudinal cross-sections of one of the four rods from each layer, all with 9.25 mm diameter, through which the highest total multimode laser power was obtained. The highest pump flux value registered in each layer is also given. The red color represents maximum pump flux of 0.323 W/mm^3, whereas blue means little or no flux.

For every rod from each layer, the maximum absorption occurs in the middle sector, as depicted in Figure **4**. Furthermore, with the increase of the layer number, the corresponding set of four rods is further away from the focal zone and the distance between the rods and the central axis of the main structure decreases. Consequently, the laser rod length also decreases, leading to a higher pumping intensity.

To understand the influence of the temperature distribution along the rod, a thermal performance analysis is necessary [33,34]. In that regard, the absorbed pump flux data from Zemax® was then processed by the LASCAD™ software to quantify the thermal effects applied in the active medium and, consequently, to optimize the solar laser output power associated with the resonator beam parameters. The design parameters of the scheme were further optimized in Zemax® based on these results.

3.2. Modeling of the Laser Resonator Parameters through LASCAD™ Software

In LASCAD™, a stimulated emission cross-section of 2.8 × 10^{-19} cm^2, a fluorescence lifetime of 230 μs [35] and a typical absorption and scattering loss of 0.003

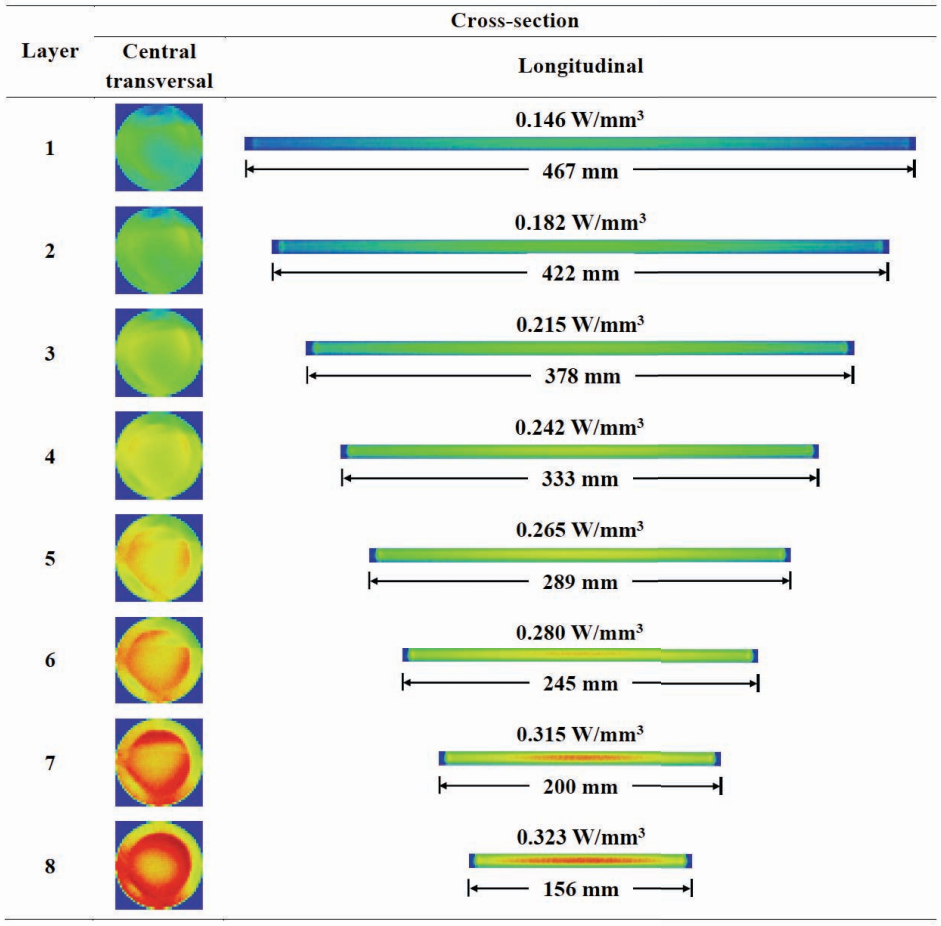

Figure 4: Absorbed pump flux distribution in the central transversal and longitudinal cross-sections of one 9.25 mm diameter rod from each of the eight layers. The highest pump flux value registered in each layer is also given. Red represents maximum pump flux of 0.323 W/mm^3, whereas blue means little or no absorption.

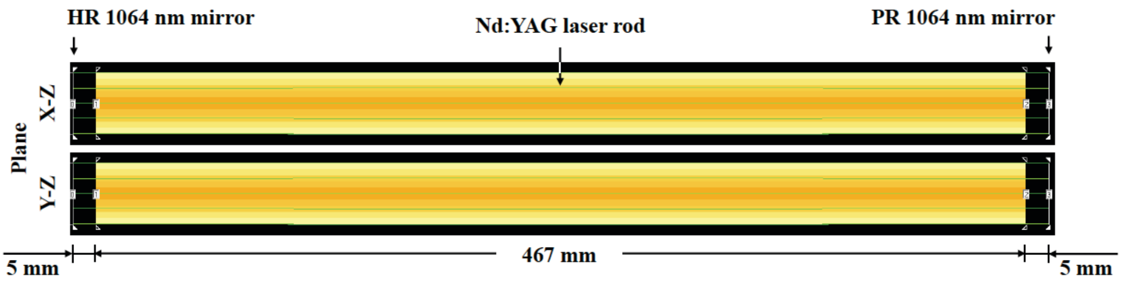

Figure 5: Laser resonator design in LASCAD™ for one of the 9.25 mm diameter Nd:YAG rods of layer 1, with a spacing of 5 mm between the rod and each mirror. Similar laser resonator designs were used in every layer to obtain maximum multimode laser power, with the only distinction being the rod length.

cm^{-1} for the 1.0 at% Nd:YAG medium were considered in the analysis. The mean absorbed and intensity-weighted solar pump wavelength of 660 nm was also used [2]. In the software, each optical resonator was comprised of two opposing mirrors, with their optical axes aligned with that of the Nd:YAG rod. The leftmost end mirror represents the HR 1064 nm mirror while the rightmost is the PR 1064 nm output coupler, with PR varying from 30% to 90%.

Figure **5** depicts the laser resonator design for one of the 9.25 mm diameter Nd:YAG rods to obtain maximum multimode laser power. A short resonator, with a spacing of 5 mm between the rod and each plane mirror, was adopted to ensure that the energy of higher order modes would not be wasted by diffraction losses.

To significantly improve the laser beam quality, the laser resonator was designed in a slightly different manner than the aforementioned one for maximum extraction of quasi-Gaussian laser beams. The resonator length was the key parameter to achieve efficient extraction of these beams due to the power-dependent thermal lensing of the laser material. The Gaussian beam has the smallest size and divergence in a resonator [35]. Consequently, for short laser resonators (Figure **5**), the Gaussian beam mode poorly matches the gain region, and laser oscillates at several modes, which comes at the expense of high M^2 factors. As the resonator length increases, the Gaussian beam size within the rod also increases and higher order modes are suppressed by large diffraction losses at the rod edges. Therefore, long resonator length was chosen (Figure **6**) at the cost of laser power losses, so that only few order modes could oscillate, thus improving beam quality [35]. Since the rod acts as an aperture, its diameter was reduced to 6 mm to facilitate the oscillation of lower order modes. Both resonator length and radius of curvature of the HR and PR mirrors were also optimized for each layer. In Figure **6**, the laser resonator design for one 6 mm diameter rod of layer 1 is shown. A detailed description of each laser resonator design for extraction of a quasi-Gaussian beam is given in Section 5.

3.3. Analytical Calculation of the Solar Laser Output Power

The laser output power (P_{out}) can be analytically calculated in terms of incoming power (P_{solar}) and measurable quantities through Equation 3 [35],

$$P_{out} = \left(\frac{1-R}{1+R}\right)\left(\frac{2\eta_{ovl}\eta_{t}\eta_{a}\eta_{q}\eta_{s}\eta_{B}}{\delta - \ln R}P_{solar} - AI_{s}\right), \quad (3)$$

where A is the cross-section area of the laser rod, I_s the saturation intensity, and R the reflectivity of the output coupler. δ defines the round-trip losses and is given by $\delta = 2\alpha l_R + L_M + L_D$. The factor $2\alpha l_R$ expresses the two-way loss inside the resonator, with α being the scattering coefficient of the laser material (= 0.003 cm^{-1}). L_M represents the miscellaneous losses related to the imperfect HR coating losses, and L_D the diffraction losses of the resonant cavity. η_{ovl} is the overlap between the laser medium absorption and

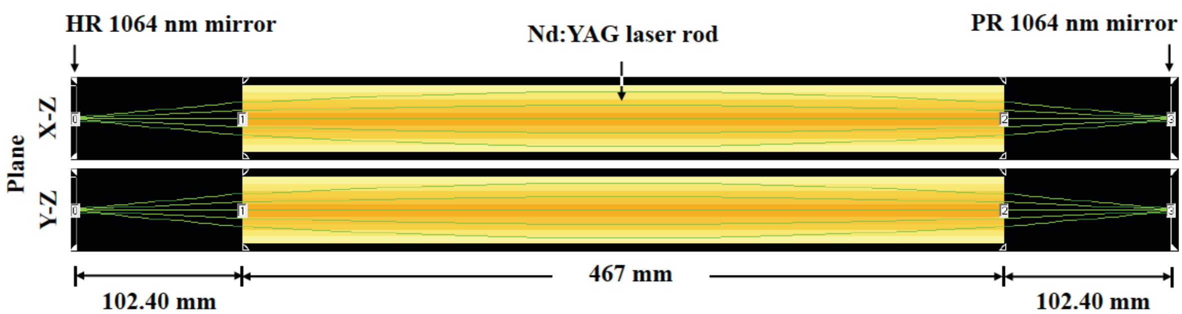

Figure 6: Laser resonator design in LASCAD™ for one of the 6 mm diameter Nd:YAG rods of layer 1, with a spacing of 102.40 mm between the rod and each mirror, for extraction of a quasi-Gaussian beam.

Table 1: Parameters Used for the Calculation of the Multimode Laser Output Power, for One 9.25 mm Diameter Nd:YAG Rod from Each of the Eight Layers

Layer	1	2	3	4	5	6	7	8
□ (cm^2)	0.672	0.672	0.672	0.672	0.672	0.672	0.672	0.672
□□ (kW/cm^2) [35]	2.9	2.9	2.9	2.9	2.9	2.9	2.9	2.9
□□ (cm)	46.7	42.2	37.8	33.3	28.9	24.5	20.0	15.6
□□□□□ (W)	2709	3182	3818	4246	4296	4049	3564	3039
□	0.75	0.73	0.69	0.67	0.67	0.70	0.72	0.77
□ (cm^{-1})	0.003	0.003	0.003	0.003	0.003	0.003	0.003	0.003
□□	0.004	0.004	0.004	0.004	0.004	0.004	0.004	0.004
□□	0.0002	0.0002	0.0002	0.0002	0.0002	0.0002	0.0002	0.0002
□□□□ [32]	0.16	0.16	0.16	0.16	0.16	0.16	0.16	0.16
□□	0.014	0.016	0.019	0.021	0.021	0.020	0.018	0.015
□□	0.83	0.84	0.84	0.84	0.84	0.84	0.84	0.84
□□ □[35]□	0.90	0.90	0.90	0.90	0.90	0.90	0.90	0.90
□□ [2]	0.62	0.62	0.62	0.62	0.62	0.62	0.62	0.62
□□	0.70	0.71	0.71	0.72	0.73	0.73	0.74	0.75
□□□□ (W)	351	459	620	749	800	773	709	613

the solar emission spectra, which is 16% for the Nd:YAG medium [32]. □□ is the fraction of useful pump radiation, which is transferred from the focus of the MWSF to the laser media. □□ is the fraction of the transferred useful radiation absorbed by the laser material. □□ and □□ are the quantum efficiency and Stokes factor, respectively. For the mean absorbed and intensity weighted pump wavelength of 660 nm, □□ = 62% was found [2]. □□ is the beam overlap efficiency, which is the spatial overlap between the resonator modes and the absorbed pump distribution within the laser medium. It was numerically obtained through LASCAD™ analysis. These parameters are summarized in Table **1**, considering the Nd:YAG rods of 9.25 mm diameter. The analytical calculation of the multimode laser output power gave a total of 20.30 kW.

It is worth noting that the analytical calculation presents only approximate values due to not relying upon the detailed absorbed pump distribution within the laser rods. By using Zemax® and LASCAD™ software, much more accurate results can be determined since the numerical analysis considers a detailed three-dimensional absorbed pump power distribution, as well as the thermal effects, within the laser rods.

4. NUMERICAL OPTIMIZATION OF THE MULTIMODE SOLAR LASER PERFORMANCE

To estimate the maximum multimode solar laser power that can be achieved by this scheme, the parameters of the biconic surfaces were initially studied, in conjunction with the distance between the rods of layer 1 and the central axis of the main structure. Both rod diameter and number of layers were then optimized, while also adjusting the internal pyramidal reflector's height and base width. Figure **7** shows the total laser power as a function of the rod diameter, for seven (N = 7), eight (N = 8) and nine (N = 9) layers.

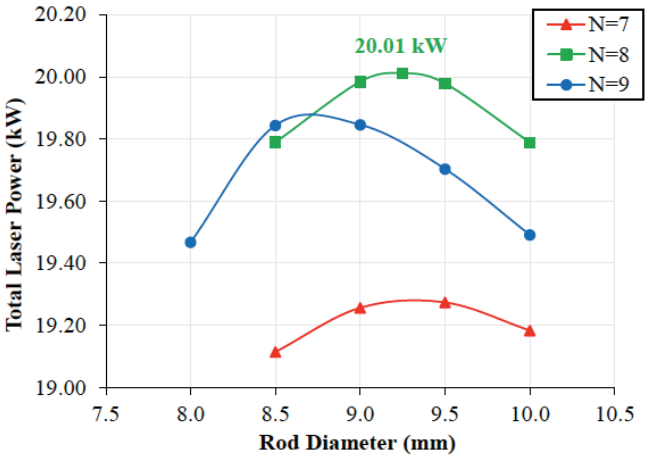

Figure 7: Numerically calculated total laser output power as a function of the rod diameter, for three different number of layers (N): 7, 8, and 9.

The incorporation of the pyramidal reflector in the multilayered structure led to a reduction of the number of layers needed to reach the system's potential. As observed in Figure **7**, total laser power of 20.01 kW was achieved with N = 8 layers, each with four rods of 9.25 mm diameter, which is similar to the 20.30 kW from the analytical calculation. With N = 7 and N = 9 layers, the highest laser output powers were 19.27 kW and 19.85 kW, obtained with rod diameters of 9.5 mm and 9 mm, respectively. It is worth noting that the

position of the highest total laser power attained shifted towards a lower rod diameter with the increase of the number of layers.

Figure **8** shows the laser power from one of the four 9.25 mm diameter rods of each layer of the N = 8 pumping cavity. Laser powers ranging from 269 W to 816 W were generated. The maximum value was obtained in layer 5 with a rod length of 289 mm, whereas a 467 mm length rod in layer 1 produced the minimum laser power.

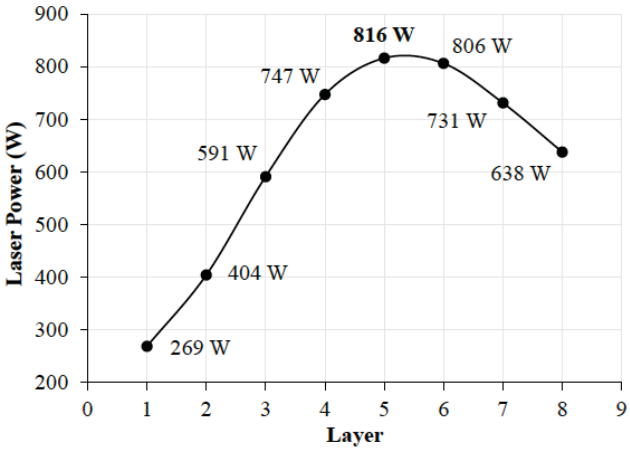

Figure 8: Numerically calculated laser output power in each of the N = 8 layers, for one 9.25 mm diameter rod.

5. IMPROVEMENT OF THE SOLAR LASER BEAM QUALITY

To enable the production of four quasi-Gaussian beams in each of the N = 8 layers, the rod diameter was reduced to 6 mm and the laser resonator design parameters were adjusted. The main structure and the pyramidal reflector remained unaltered, while the inner diameter of each flow tube was reduced to maintain the cross-section area of 30 mm^2 used for the circulation of cooling water. In Figure **9**, the laser resonator design for one 6 mm diameter Nd:YAG rod from each of the N = 8 layers is presented, as well as the resultant laser beam profile. The numerically calculated laser output power and laser beam quality factors M_x^2 and M_y^2 are also shown.

Since the rod length is different in each layer, HR and PR mirrors of different radii of curvature were used, along with different spacings between the laser rod and each mirror, in order to obtain quasi-Gaussian beam profiles in each case. A longer symmetric cavity provided better results overall.

The quasi-Gaussian laser beam power rose with the increase of the layer number until layer 6, where maximum laser power of 425 W was numerically achieved from each of the four 6 mm diameter, 245 mm length Nd:YAG rods. After that, a decrease of laser power occurred (Figure **9**). The minimum laser power of 131 W was numerically obtained from each of the four rods with longer length (467 mm), in layer 1. A total laser power of 9.44 kW was attained. The thermal lensing was also progressively more pronounced with the layer number until layer 4, leading to a decrease in the thermal focal lens, while the opposite happened subsequently. Considerable enhancement of the M_x^2 M_y^2 beam quality factors and, consequently, the laser beam quality was achieved in every layer. Nearly symmetric M_x^2 M_y^2 factors were obtained due to the usage of convex resonator mirrors with low radius of curvature, which helped in the improvement of the quasi-Gaussian beam profiles.

6. CONCLUSIONS

An alternative multirod solar laser station concept for the production of multiple quasi-Gaussian beams in a Megawatt solar furnace was proposed, composed of an eight-layered structure that contained four laser heads in each layer. Once the overall shape of the main structure was optimized, the influence of the number of layers and rod diameter on the laser power was studied. The most efficient rod pumping configuration was found by side-pumping eight layers of four rods each, whose length varied depending on which layer they were part of.

This scheme provided alleviation of the thermal lensing effects and considerable improvement of the laser beam quality, when compared to another concept that utilizes the same solar facility [27]. With 6 mm diameter rods, this may ensure the generation of 9.44 kW total laser power through multiple laser beams with quasi-Gaussian profiles, which could become a valuable asset for a vast assortment of laser-based applications in solar energy research. Moreover, total multimode laser power of 20.01 kW was numerically determined by using 9.25 mm diameter rods. This corresponds to a 10.93 W/m^2 collection efficiency and a 2.0% solar-to-laser power conversion efficiency, with the latter representing a 1.54 times enhancement over the 1.3% of the scheme with the MWSF in Uzbekistan [22], which consisted in the side-pumping of five Nd:YAG rods.

Since a solar laser is pumped by a nearly eternal and free power source, the 20 kW-class solar laser station can avoid using many expensive semiconductor laser stacks with lifetimes of only 2 - 3 years, enabling reliable renewable laser operation over a multitude of years. Economically, when compared to electrically pumped lasers, solar pumping offers considerable design simplicity and cost competitiveness due to the complete elimination of expensive electrical power generation and conditioning units. In addition to its cost advantage, other potential benefits of solar lasers

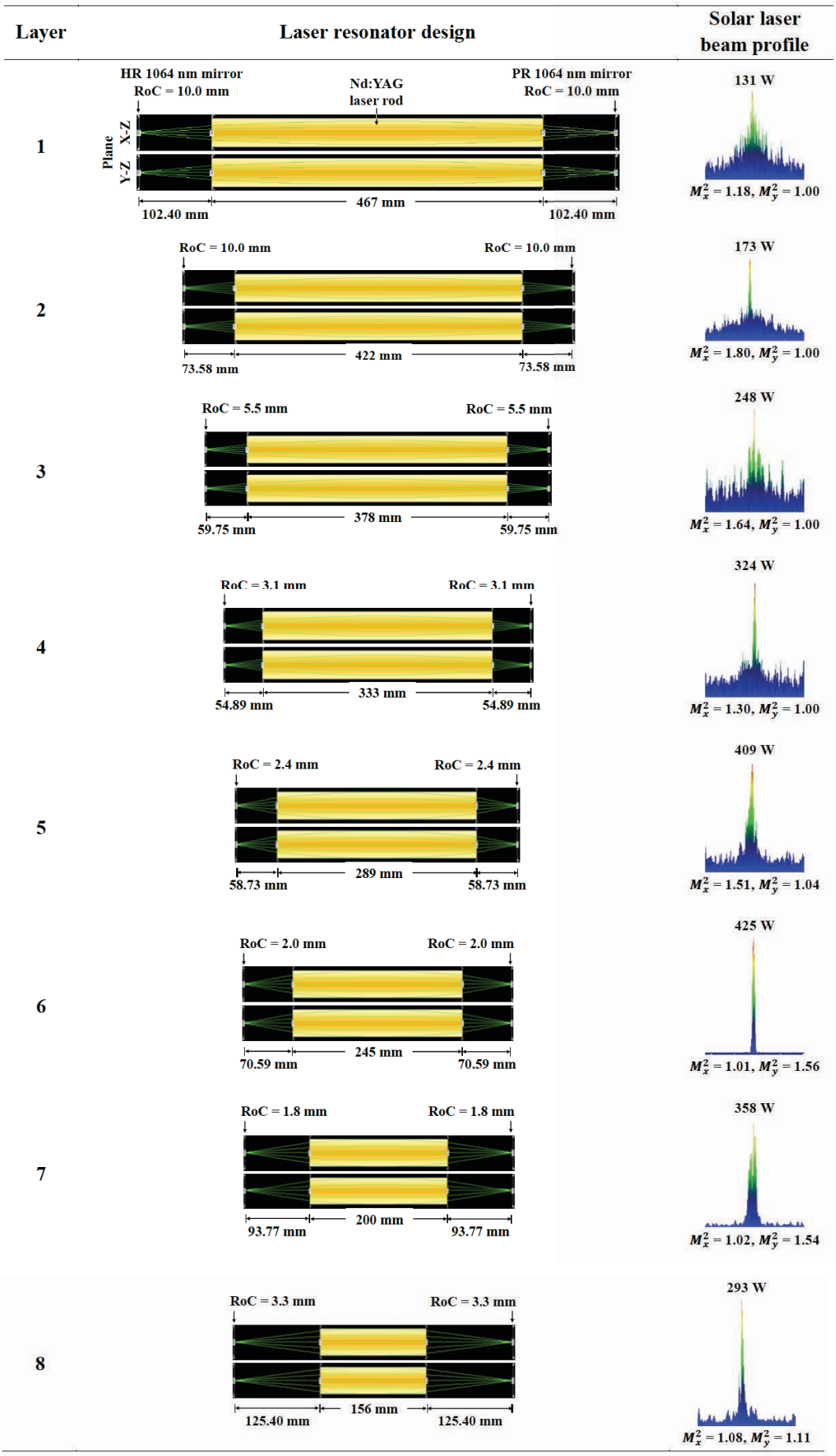

Figure 9: Laser resonator design in LASCAD™ for one of the 6 mm diameter Nd:YAG rods from each of the N = 8 layers and resultant quasi-Gaussian solar laser beam profiles, with the numerically calculated laser output powers and beam quality factors M_x^2 and M_y^2. RoC represents the radius of curvature of the laser resonator mirrors.

include improved reliability and lifetime, increased overall efficiency, reduced laser system complexity, and retrenchment on system level (power supply, heat removal, redundancy).

ACKNOWLEDGEMENTS

Financial support of the strategic project (UIDB/00068/2020) of the Science and Technology Foundation of Portuguese Ministry of Science, Technology and Higher Education (FCT-MCTES) is acknowledged. The contract CEECIND/03081/2017 and the fellowship grants PD/BD/128267/2016, PD/BD/142827/2018, SFRH/BD/145322/2019 and SFRH/BPD/125116/2016 of Joana Almeida, Bruno D. Tibúrcio, Dário Garcia, Miguel Catela, and Cláudia R. Vistas, respectively, are also acknowledged.

ABBREVIATIONS

HR	=	Highly reflective
LASCAD	=	Laser cavity analysis and design
MWSF	=	One-Megawatt solar furnace
N	=	Number of layers
PR	=	Partially reflective
PROMES-CNRS	=	Procédés, Matériaux et Energie Solaire – Centre National de la Recherche Scientifique
RoC	=	Radius of curvature of the laser resonator mirrors

REFERENCES

[1] Rather JDG, Gerry ET, Zeiders GW. Investigation of possibilities for solar powered high energy lasers in space. NASA Tech Reports Serv 1977;

[2] Weksler M, Shwartz J. Solar-pumped solid-state lasers. IEEE J Quantum Electron [Internet] 1988 Jun; 24(6): 1222-8. Available from: https://ieeexplore.ieee.org/document/247/

[3] Vasile M, Maddock CA. Design of a formation of solar pumped lasers for asteroid deflection. Adv Sp Res [Internet] 2012 Oct; 50(7): 891-905. http://dx.doi.org/10.1016/j.asr.2012.06.001

[4] Yabe T, Uchida S, Ikuta K, Yoshida K, Baasandash C, Mohamed MS, *et al*. Demonstrated fossil-fuel-free energy cycle using magnesium and laser. Appl Phys Lett [Internet] 2006 Dec 25; 89(26): 261107. Available from: http://aip.scitation.org/doi/10.1063/1.2423320

[5] Oliveira M, Liang D, Almeida J, Vistas CR, Gonçalves F, Martins R. A path to renewable Mg reduction from MgO by a continuous-wave Cr: Nd: YAG ceramic solar laser. Sol Energy Mater Sol Cells [Internet] 2016 Oct; 155: 430-5. https://doi.org/10.1016/j.solmat.2016.06.046

[6] Kiss ZJ, Lewis HR, Duncan Jr. RC. Sun Pumped Continuous Optical Maser. Appl Phys Lett [Internet] 1963; 2(5): 93-4. https://doi.org/10.1063/1.1753794

[7] Maiman TH. Stimulated Optical Radiation in Ruby. Nature [Internet] 1960 Aug; 187(4736): 493-4. Available from: http://www.nature.com/articles/187493a0

[8] Young CG. A Sun-Pumped cw One-Watt Laser. Appl Opt [Internet] 1966 Jun 1; 5(6): 993. https://doi.org/10.1364/AO.5.000993

[9] Arashi H, Oka Y, Sasahara N, Kaimai A, Ishigame M. A Solar-Pumped cw 18 W Nd: YAG Laser. Jpn J Appl Phys [Internet] 1984 Aug 20; 23(Part 1, No. 8): 1051-3. Available from: http://stacks.iop.org/1347-4065/23/1051

[10] Lando M, Kagan J, Linyekin B, Dobrusin V. A solar-pumped Nd: YAG laser in the high collection efficiency regime. Opt Commun [Internet] 2003 Jul; 222(1-6): 371-81. https://doi.org/10.1016/S0030-40180301601-8

[11] Jenkins D, Lando M, Winston R, O'Gallagher J. A solar-pumped Nd: YAG laser with a record efficiency of 4.7 watt/m^2 of primary mirror area. Bull Isr Phys Soc 1996; 42(101).

[12] Liang D, Vistas CR, Tibúrcio BD, Almeida J. Solar-pumped Cr: Nd: YAG ceramic laser with 6.7% slope efficiency. Sol Energy Mater Sol Cells [Internet] 2018 Oct; 185(March): 75-9. https://doi.org/10.1016/j.solmat.2018.05.020

[13] Yabe T, Ohkubo T, Uchida S, Yoshida K, Nakatsuka M, Funatsu T, *et al*. High-efficiency and economical solar-energy-pumped laser with Fresnel lens and chromium codoped laser medium. Appl Phys Lett [Internet] 2007 Jun 25; 90(26): 261120. https://doi.org/10.1063/1.2753119

[14] Liang D, Almeida J. Highly efficient solar-pumped Nd: YAG laser. Opt Express [Internet] 2011 Dec 19; 19(27): 26399. https://doi.org/10.1364/OE.19.026399

[15] Dinh TH, Ohkubo T, Yabe T, Kuboyama H. 120 watt continuous wave solar-pumped laser with a liquid light-guide lens and an Nd: YAG rod. Opt Lett [Internet] 2012 Jul 1; 37(13): 2670. https://doi.org/10.1364/OL.37.002670

[16] Almeida J, Liang D, Guillot E. Improvement in solar-pumped Nd: YAG laser beam brightness. Opt Laser Technol [Internet] 2012 Oct; 44(7): 2115-9. https://doi.org/10.1016/j.optlastec.2012.03.017

[17] Almeida J, Liang D, Guillot E, Abdel-Hadi Y. A 40 W cw Nd: YAG solar laser pumped through a heliostat: a parabolic mirror system. Laser Phys [Internet] 2013 Jun 1; 23(6): 065801. https://doi.org/10.1088/1054-660X/23/6/065801

[18] Xu P, Yang S, Zhao C, Guan Z, Wang H, Zhang Y, *et al*. High-efficiency solar-pumped laser with a grooved Nd: YAG rod. Appl Opt [Internet] 2014 Jun 20; 53(18): 3941. https://doi.org/10.1364/AO.53.003941

[19] Liang D, Almeida J, Vistas CR, Guillot E. Solar-pumped Nd: YAG laser with 31.5 W/m^2 multimode and 7.9 W/m^2 TEM_{00}-mode collection efficiencies. Sol Energy Mater Sol Cells [Internet] 2017 Jan; 159: 435-9. https://doi.org/10.1016/j.solmat.2016.09.048

[20] Guan Z, Zhao C, Li J, He D, Zhang H. 32.1 W/m^2 continuous wave solar-pumped laser with a bonding Nd: YAG/YAG rod and a Fresnel lens. Opt Laser Technol [Internet] 2018 Nov; 107: 158-61. https://doi.org/10.1016/j.optlastec.2018.05.039

[21] Hwang IH, Lee JH. Efficiency and threshold pump intensity of CW solar-pumped solid-state lasers. IEEE J Quantum Electron [Internet] 1991; 27(9): 2129-34. Available from: http://ieeexplore.ieee.org/document/135171/

[22] Fazilov A, Riskiev TT, Abdurakhmanov AA, Bakhramov SA, Makhkamov S, Mansurov MM, *et al*. Concentrated solar energy conversion to powerful laser radiation on neodymium activated yttrium-aluminum garnet. Appl Sol Energy [Internet] 2008 Jun 22; 44(2): 93-6. Available from: http://link.springer.com/10.3103/S0003701X08020072

[23] Tibúrcio BD, Liang D, Almeida J, Garcia D, Vistas CR. Dual-rod pumping concept for TEM_{00}-mode solar lasers. Appl Opt [Internet] 2019 May 1; 58(13): 3438. https://doi.org/10.1364/AO.58.003438

[24] Almeida J, Liang D, Tibúrcio BD, Garcia D, Vistas CR. Numerical modeling of a four-rod pumping scheme for improving TEM_{00}-mode solar laser performance. J Photonics Energy [Internet] 2019 Feb 20; 9(01): 1. https://doi.org/10.1117/1.JPE.9.018001

[25] Liang D, Almeida J, Garcia D, Tibúrcio BD, Guillot E, Vistas CR. Simultaneous solar laser emissions from three Nd: YAG rods within a single pump cavity. Sol Energy [Internet] 2020 Mar; 199: 192-7. https://doi.org/10.1016/j.solener.2020.02.027

[26] Almeida J, Liang D, Costa H, Garcia D, Tibúrcio BD, Catela M, *et al*. Seven-rod pumping concept for simultaneous emission of seven TEM_{00}-mode solar laser beams. J Photonics Energy [Internet] 2020; 10(3): 038001. https://doi.org/10.1117/1.JPE.10.038001

[27] Costa H, Almeida J, Liang D, Garcia D, Catela M, Tibúrcio BD, *et al*. Design of a multibeam solar laser station for a megawatt solar furnace. Opt Eng [Internet] 2020; 59(8): 086103. https://doi.org/10.1117/1.OE.59.8.086103

[28] Guillot E, Rodriguez R, Boullet N, Sans J-L. Some details about the third rejuvenation of the 1000 kWth solar furnace in Odeillo: Extreme performance heliostats. In: AIP Conference Proceedings [Internet] 2018. p. 040016. Available from: http://aip.scitation.org/doi/abs/10.1063/1.5067052

[29] SFERA. Access to PROMES facilities [Internet]. [cited 2020 May 6]. Available from: http://sfera.sollab.eu/index.php?page=access_promes

[30] Lupei V, Lupei A, Gheorghe C, Ikesue A. Emission sensitization processes involving Nd^{3+} in YAG. J Lumin [Internet] 2016 Feb; 170: 594-601. http://dx.doi.org/10.1016/j.jlumin.2015.04.045

[31] ASTM G173-03(2012), Standard Tables for Reference Solar Spectral Irradiances: Direct Normal and Hemispherical on 37° Tilted Surface. West Conshohocken, PA: ASTM International; 2012.

[32] Zhao B, Changming Z, He J, Yang S. The study of active medium for solar-pumped solid-state lasers. Acta Opt Sin 2007; 27(10): 1797-1801.

[33] Turkyilmazoglu M. Heat transfer from warm water to a moving foot in a footbath. Appl Therm Eng [Internet] 2016 Apr; 98: 280-7. http://dx.doi.org/10.1016/j.applthermaleng.2015.12.027

[34] Turkyilmazoglu M. Thermal management of parabolic pin fin subjected to a uniform oncoming airflow: optimum fin dimensions. J Therm Anal Calorim [Internet] 2021 Mar 19; 143(5): 3731-9. https://doi.org/10.1007/s10973-020-10382-x

[35] Koechner W. Solid-State Laser Engineering [Internet]. 5th ed. Springer-Verlag Berlin Heidelberg; 1999. (Springer Series in Optical Sciences). https://doi.org/10.1007/978-3-662-14219-6

Received on 14-01-2021 Accepted on 26-02-2021 Published on 26-03-2021

DOI: https://doi.org/10.31875/2410-2199.2021.08.02